

Article

Thermoelectric and Magnetic Properties and Electronic Structure of Solid Solutions $\text{CuCr}_{1-x}\text{La}_x\text{S}_2$

Evgeniy V. Korotaev * , Mikhail M. Syrokvashin  and Irina Yu. Filatova

Nikolaev Institute of Inorganic Chemistry, Siberian Branch, Russian Academy of Sciences, 630090 Novosibirsk, Russia; syrokvashin@niic.nsc.ru (M.M.S.); rare@niic.nsc.ru (I.Y.F.)

* Correspondence: korotaev@niic.nsc.ru

Abstract: The oxidation states of atoms in $\text{CuCr}_{1-x}\text{La}_x\text{S}_2$ ($x = 0\text{--}0.03$) solid solutions were determined using the analysis of Cu2p, Cr2p, S2p, and La3d core level binding energy. The cationic substitution did not significantly affect the charge distribution on matrix elements (Cu, Cr, and S). The oxidation states of the atoms were identified as S^{2-} for sulfur, Cu^+ for copper, and Cr^{3+} for chromium. The cationic substitution in $\text{CuCr}_{1-x}\text{La}_x\text{S}_2$ was found to occur via the isovalent principle. The cationic substitution of CuCrS_2 matrix with lanthanum ions led to the enhancement of the Seebeck coefficient comparing $\text{CuCr}_{1-x}\text{La}_x\text{S}_2$ to the initial matrix. The observed enhancement was attributed to the reconstruction of the valence band electronic structure after the cationic substitution. The maximum Seebeck coefficient value of 412 $\mu\text{V}/\text{K}$ was measured for $\text{CuCr}_{0.985}\text{La}_{0.015}\text{S}_2$ at 420 K. An increase in the lanthanum concentration to $x = 0.03$ caused a suppression of the Seebeck coefficient. The synthetic route was found to significantly affect both the magnetic properties and charge carrier concentration. The magnetic properties of $\text{CuCr}_{1-x}\text{La}_x\text{S}_2$ synthesized using metal sulfide reagents cannot be interpreted using the simple isovalent Cr^{3+} to La^{3+} cationic substitution model. The defectiveness of the samples and the formation of the impurity CuLaS_2 phase could be additional factors that affect the magnetic properties of $\text{CuCr}_{1-x}\text{La}_x\text{S}_2$.

Keywords: layered copper-chromium disulfide; lanthanides; XPS; electronic structure; static magnetochemistry; Seebeck coefficient; thermoelectric materials



Citation: Korotaev, E.V.; Syrokvashin, M.M.; Filatova, I.Y. Thermoelectric and Magnetic Properties and Electronic Structure of Solid Solutions $\text{CuCr}_{1-x}\text{La}_x\text{S}_2$. *J. Compos. Sci.* **2023**, *7*, 436. <https://doi.org/10.3390/jcs7100436>

Academic Editor: Aleksey A. Vedyagin

Received: 15 September 2023

Revised: 29 September 2023

Accepted: 11 October 2023

Published: 13 October 2023



Copyright: © 2023 by the authors. Licensee MDPI, Basel, Switzerland. This article is an open access article distributed under the terms and conditions of the Creative Commons Attribution (CC BY) license (<https://creativecommons.org/licenses/by/4.0/>).

1. Introduction

Rapid technical progress demands the development of advanced functional materials and the improvement of the properties of existing materials through a series of research progress. In this context, multipurpose functional materials such as graphene, carbon nanotubes, and layered compounds based on transition metal chalcogenides are of special interest. Layered copper-chromium disulfide CuCrS_2 - and CuCrS_2 -based cation-substituted solid solutions can be considered as multipurpose advanced functional materials. These compounds exhibit various promising functional properties and effects, including thermoelectricity [1–7], ionic conductivity [8–10] and the order-to-disorder transition (ODT) [9,11–13], magnetoresistance [14,15] and the metal-to-insulator transition (MIT) [14,16], helimagnetic arrangement [17–19], light-absorbing [20] and luminescence properties [21], and ferroelectricity [22,23]. The combination of functional properties in CuCrS_2 -based solid solutions makes them promising materials for the fabrication of various electronic devices, including temperature sensors, thermoelectric generators (TEGs) [2,5–7,24], solid-state current sources [8,9], magnetic field sensors [14], solid-state memory [18,22,23], and electric or magnetic-field-driven valves [14,22,23].

The thermoelectric properties of CuCrS_2 -based compounds are of special interest due to the presence of ionic conductivity. The combination of thermoelectric and superionic properties allows one to consider these compounds as phonon liquid electronic crystal (PLEC) materials. PLEC materials, such as sulfide- or selenide-based compounds, possess

a high Seebeck coefficient. This is due to the fact that these compounds have a *fixed* crystal matrix, resulting in low thermal conductivity related to the presence of mobile cations effectively scattering the phonons [25–31]. In the case of CuCrS₂-based solid solutions, the chromium sublattice formed by the -S-Cr-S- layers can be considered as the “*fixed*” crystal matrix. At high temperatures, the mobile copper cations can migrate between different crystallographic sites in the copper sublattice and, thereby, can be considered as a *phonon liquid* [9,12,17]. The cationic substitution of the matrix elements (Cu, Cr or S) affects the Seebeck coefficient and ionic conductivity of CuCrS₂-based compounds [3,9,10,32–36]. The cationic substitution of Cr atoms in the low-dopant concentration range ($x < 0.03$) increases both the Seebeck coefficient value and the ionic conductivity of CuCr_{1-x}M_xS₂ solid solutions (M—transition metal or lanthanide atom) [3,33,35,36]. A systematic study focused on the thermoelectric properties and electronic structure of lanthanide-doped CuCr_{0.99}Ln_{0.01}S₂ solid solutions revealed a notable enhancement in the Seebeck coefficient value after cationic substitution [32,33,35,36]. The most significant enhancement of the thermoelectric properties was reported for the La-doped CuCr_{1-x}La_xS₂ solid solutions [33,35,36]. Note that the Seebeck coefficient can be considered as one of the key parameters of the efficient thermoelectric materials used in temperature sensors and TEGs [37]. The critical analysis of the reported data concerning the study of functional properties of CuCrS₂-based solid solutions indicates that the synthesis route and sample treatment significantly impact the thermoelectric, electrophysical, and magnetic properties of these materials [1,3,4,14,16,21,38–41]. For instance, the overwhelming majority of the reported studies were carried out on samples synthesized using commercial metal oxides as the initial reagents to obtain CuCrS₂-matrix and CuCrS₂-based solid solutions [3,32–34,39]. In particular, the series of the lanthanum-substituted solid solutions CuCr_{1-x}La_xS₂ ($x = 0–0.03$) was previously obtained and characterized using powder X-ray diffraction, static magnetochemistry, Seebeck coefficient, and Hall voltage measurements [42]. However, the final synthesis product had an additional impurity CuLaS₂ phase in the high-dopant-concentration region for CuCr_{1-x}La_xS₂ ($x > 0.01$) solid solutions. The presence of the impurity phase affected both the thermoelectric and magnetic properties of CuCr_{1-x}La_xS₂ solid solutions. In this regard, it was suggested to vary the initial reagent compounds and study their influence on the formation of CuLaS₂ phase in the final synthesis products and, therein, the thermoelectric and magnetic properties of CuCr_{1-x}La_xS₂ ($x = 0–0.03$) solid solutions.

2. Experimental

The initial sulfide reagents Cr₂S₃ and La₂S₃ were synthesized using commercial metal oxides Cr₂O₃ and La₂O₃ with a purity of 99.99%. The metal oxide powder in a glassy carbon boat was placed in a horizontal high-temperature quartz tube furnace. The sulfidation of the oxide powder was carried out with the gaseous decomposition products of NH₄SCN at a temperature of 1050°C. High-purity argon gas was used as the carrier gas. During the sulfidation procedure, the product was ground for several times. The completeness of sulfidation was controlled at each grinding stage through powder X-ray diffraction (XRD) using a non-monochromatic CuK α X-ray radiation source ($\lambda = 1.5406 \text{ \AA}$) on a Bruker D8 Advance diffractometer (Bruker, Berlin, Germany). Then, using the synthesized sulfide powders of Cr₂S₃, La₂S₃, and the commercial Cu₂S with a purity of 99.99%, the final CuCr_{1-x}La_xS₂ ($x = 0, 0.005, 0.01, 0.015, \text{ and } 0.03$) products were synthesized. The synthesis route was the same as for the preparation of the initial sulfide powders. The phase composition and the formation of the final CuCr_{1-x}La_xS₂ product were analyzed using XRD.

The X-ray photoelectron spectroscopy (XPS) study of CuCr_{1-x}La_xS₂ was conducted using an ESCALAB 220i spectrometer (Thermo Fisher Scientific, Kingfisher, UK). The XPS lines of copper (Cu2p), lanthanum (La3d), and sulfur (S2p) were recorded at room temperature with a non-monochromatic AlK α X-ray source ($h\nu = 1486.6 \text{ eV}$). The chromium (Cr2p) lines were recorded using a non-monochromatic MgK α X-ray source ($h\nu = 1253.6 \text{ eV}$). The sample was fixed on a substrate using double-sided adhesive conductive carbon tape. The energy scale of the spectrometer was calibrated based on the line positions of metallic gold

Au4f_{7/2} (84.0 eV) and copper Cu2p_{3/2} (932.6 eV). The measured binding energy (BE) values were corrected using the carbon C1s-line (284.8 eV) corresponding to adventitious carbon atoms in the near-surface layers of the samples. The XPS data were processed using a CasaXPS 2.3.15 software [43]. The measurement accuracy of BE values was of 0.2 eV.

The magnetic properties of CuCr_{1-x}La_xS₂ were investigated over an extended temperature range of 80–750 K using a Faraday balance-type experimental setup. A powder sample of ~20 mg in an open-type quartz cucurbit was placed in the measurement cell volume. Subsequently, the system was evacuated to a pressure of 0.01 Torr. Following this, the measurement cell was filled with helium to a pressure of 5 Torr. The temperature within the measurement cell volume was maintained using a Delta DTB9696 temperature controller. The voltage generated by the torsion-type quartz microbalance was measured using a high-precision digital 6½ Keysight 34465 A voltmeter (Keysight Technologies, Santa-Rosa, CA, USA). The magnetic susceptibility data were treated using the additive Pascal scheme. The potential presence of ferromagnetic impurities was controlled by the inverse field dependence of the magnetic susceptibility χ (1/H). The effective magnetic moment was calculated as follows:

$$\mu_{eff}(T) \approx \sqrt{8 \cdot \chi T}$$

The temperature dependence of the Seebeck coefficient for CuCr_{1-x}La_xS₂ was measured using a self-designed experimental setup. The ceramic samples were prepared by compressing the synthesized powder under a uniaxial pressure of 70 MPa for 2 h in a vacuum of 5×10^{-5} Torr at 923 K. The ceramic sample was positioned within the measurement cell, precisely situated between copper contact pads equipped with integrated 50 W nichrome wire heaters. Then, the measurement cell was evacuated and subsequently filled with helium with a pressure of 5 Torr. The thermoelectric power generated by the sample was measured using a 6½ Keysight 34465 A voltmeter (Keysight Technologies, Santa-Rosa, CA, USA). The experimental setup was validated using a constantan reference sample of thermocouple grade. The temperature of the contact pads was maintained by a Thermodat-13K5 temperature controller (LLC RPE Control Systems, Perm, Russia) using a platinum RTD sensor. During the measurements, the direction of the temperature gradient was systematically altered as +5, 0, and –5 K. Thus, the total Seebeck coefficient value was calculated as a slope of the voltage generated by the sample as a function of the temperature gradient.

Hall voltage measurements were conducted at ambient room temperature using the Van der Pauw technique. A direct current (DC) magnetic field of 1 T was applied perpendicularly to both the direction of the electrical current and the sample plane. A current of 10 mA was passed through the sample. The Hall voltage was measured using a 6½ Keysight 34465 A voltmeter. Throughout the measurement procedure, a systematic reversal of magnetic field polarity and current direction was carried out, followed by a subsequent interchange of the current and potential measurement probes. The Hall voltage value was determined through eight independent measurements. The polarity of the Hall voltage was calibrated using reference samples of *n*- and *p*-type silicon wafers.

3. Results and Discussion

The XRD data for the powder samples studied are plotted in Figure 1. The solid solutions CuCr_{1-x}La_xS₂ synthesized using the initial sulfide reagents and the initial CuCrS₂ matrix are isostructural (*R3m* space group). The XRD data are consistent with the reference data for CuCrS₂ of the ICSD database [44]. However, the additional weak diffraction peak at 23.6° could be observed for the CuCr_{0.97}La_{0.03}S₂ solid solution (marked with * symbol in Figure 1). The corresponding diffraction peak was attributed previously to CuLaS₂ impurity phase for the samples obtained using initial metal oxide reagents [42]. Note that the corresponding peak in [42] occurred in the solid solutions with a lower lanthanum concentration range ($x > 0.01$). Thus, one can conclude that the solubility limit of La in CuCrS₂-matrix is 1.5 at.% greater than it was previously suggested in [42]. However, the lattice parameters increased for solid solutions with $x \leq 0.01$ and decreased at a higher

lanthanum concentration range (Table 1). Thus, one can conclude that the first trend is related to the isovalent cationic substitution of Cr^{3+} with La^{3+} , while the second trend corresponds to the formation of CuLaS_2 phase [42]. Consequently, the formation of CuLaS_2 phase also occurred at $x \geq 0.01$. Note that the absence of the diffraction peak of LaCrS_2 for $\text{CuCr}_{0.985}\text{La}_{0.015}\text{S}_2$ solid solution could be due to the low concentration of the impurity phase. The pure CuLaS_2 phase was additionally synthesized as the reference sample for XPS measurements. The XRD data for CuLaS_2 synthesized powder sample is depicted in Figure 1. The obtained CuLaS_2 sample consisted of particles with different space groups ($P2_1/c$, $P112_1/b$, and $P6_3$) [42]. However, the $P2_1/c$ phase was prevalent.

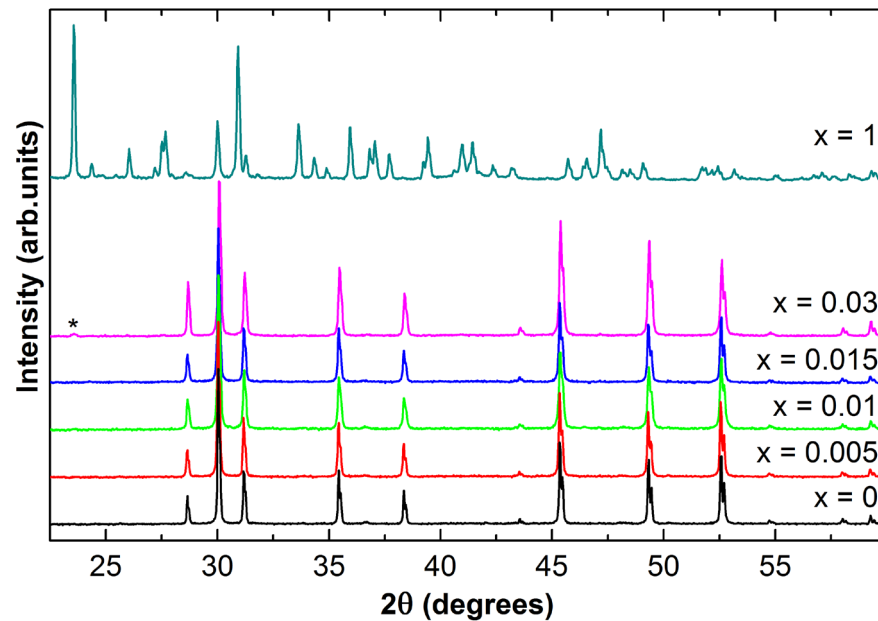


Figure 1. XRD patterns for $\text{CuCr}_{1-x}\text{La}_x\text{S}_2$ powder samples. *—most intense peak of CuLaS_2 impurity phase.

Table 1. The lattice parameters calculated for $\text{CuCr}_{1-x}\text{La}_x\text{S}_2$.

	a , Å	c , Å
CuCrS_2	3.4807(9)	18.701(6)
$\text{CuCr}_{0.995}\text{La}_{0.005}\text{S}_2$	3.4816(8)	18.707(6)
$\text{CuCr}_{0.99}\text{La}_{0.01}\text{S}_2$	3.4820(8)	18.708(6)
$\text{CuCr}_{0.985}\text{La}_{0.015}\text{S}_2$	3.4807(9)	18.702(6)
$\text{CuCr}_{0.97}\text{La}_{0.03}\text{S}_2$	3.478(1)	18.689(6)

The oxidation state of atoms in complex chemical compounds is an important parameter of particular interest. This is due to the fact that besides the electronic density distribution, the oxidation state is related to magnetic properties, magnetoresistance, and luminescence [14,45,46]. Furthermore, the oxidation state of dopant atoms affects the carrier concentration. For instance, if the oxidation state of dopant atoms is lower (or higher) compared to matrix atoms, thereby, the concentration of electrons (or holes) could be increased. X-ray photoelectron spectroscopy (XPS) is one of the most effective physical methods providing data on the oxidation state of atoms. The binding energy (BE) of core levels is related to the charge localized on the investigated atom [47]. Therefore, XPS allows one to selectively study the oxidation state of elements, even in the case of complex multi-element compounds such as CuCrS_2 -based solid solutions [41].

The XPS core level regions of copper, chromium, lanthanum, and sulfur in $\text{CuCr}_{1-x}\text{La}_x\text{S}_2$ solid solutions and CuLaS_2 impurity phase are plotted in Figures 2 and 3. The measured BEs of $\text{Cu}2p$ -, $\text{Cr}2p$ -, $\text{S}2p$ -, and $\text{La}3d$ -lines are listed in Table 2.

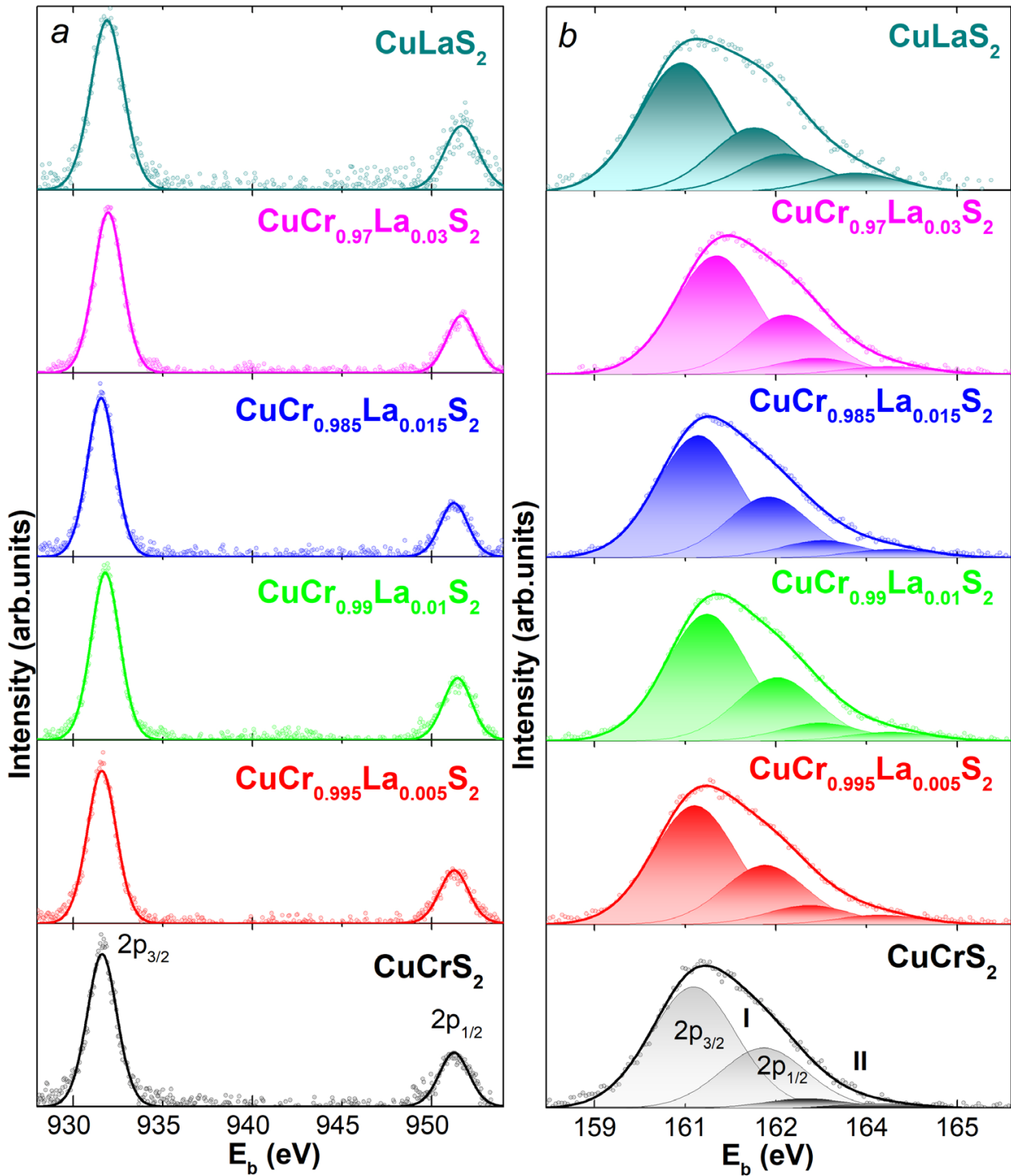


Figure 2. XPS lines for $\text{CuCr}_{1-x}\text{La}_x\text{S}_2$ and CuLaS_2 : (a) $\text{Cu}2p$ and (b) $\text{S}2p$ region.

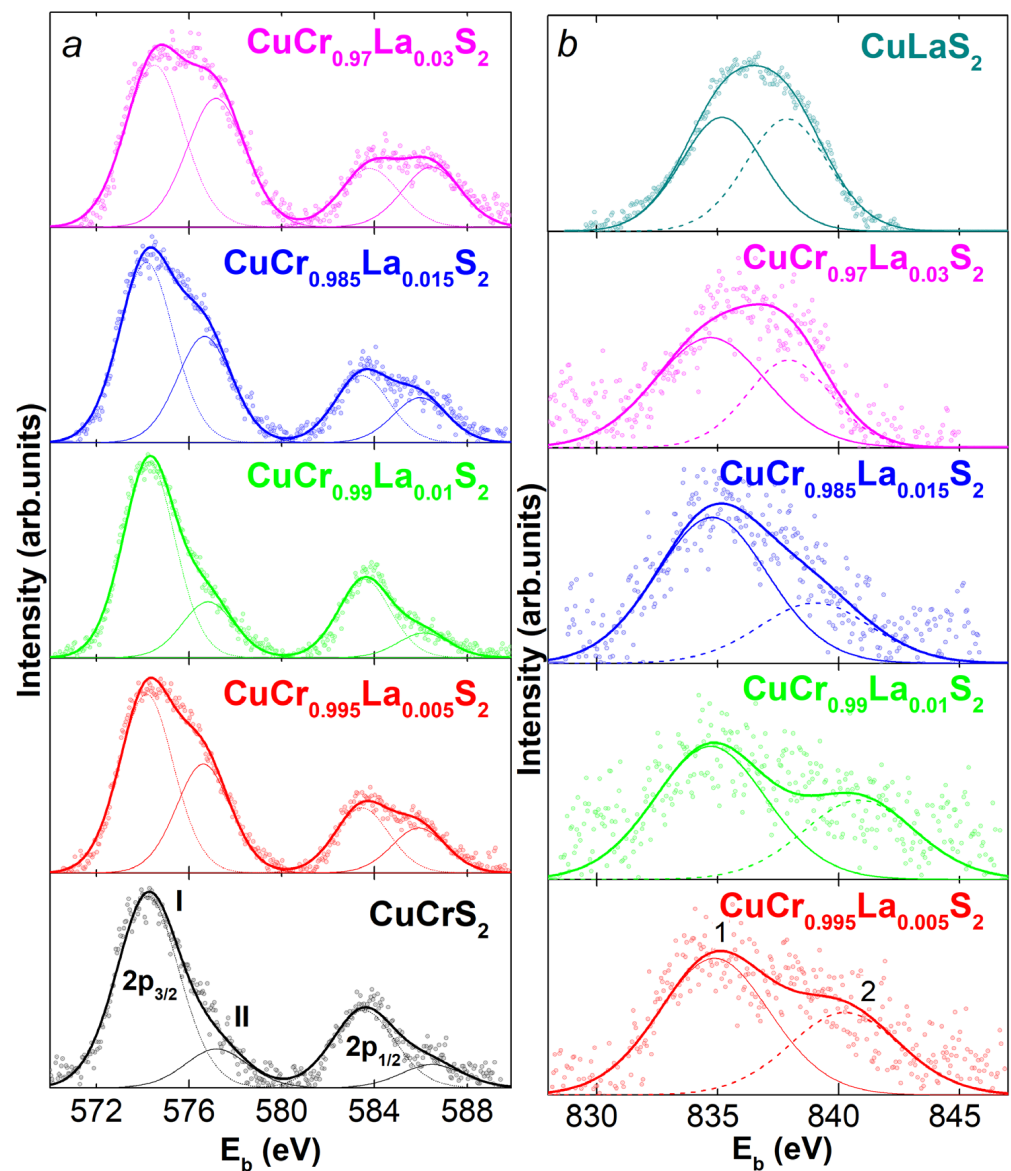


Figure 3. XPS lines for $\text{CuCr}_{1-x}\text{Ln}_x\text{S}_2$ and CuLaS_2 : (a) Cr2p- and (b) La3d-region.

Table 2. BE values for Cu2p-, Cr2p-, S2p-, and La3d-lines.

	Cu2p _{3/2}	Cr2p _{3/2}	S2p _{3/2}	La3d _{5/2}
CuCrS ₂	931.6	574.2 577.2	160.6 162.5	–
CuCr _{0.995} La _{0.005} S ₂	931.6	574.2 576.6	160.7 162.6	834.9
CuCr _{0.99} La _{0.01} S ₂	931.8	574.3 576.8	160.9 162.7	834.7
CuCr _{0.985} La _{0.015} S ₂	931.6	574.2 576.7	160.7 162.8	834.8
CuCr _{0.97} La _{0.03} S ₂	932.0	574.5 577.1	161.0 162.7	834.7
CuLaS ₂	931.9	–	160.4 162.1	835.2

The Cu2p-region is represented by two intense lines related to the spin-orbit splitting of the Cu2p-level to Cu2p_{3/2}- and Cu2p_{1/2}-sublevels (Figure 2a). Note that the intense satellite lines at ~940 eV, which were previously observed for CuCr_{0.99}Ln_{0.01}S₂ synthesized from the oxide reagents [33,35,36], are absent in the Cu2p-region of the samples studied. The presence of the satellites is the characteristic feature that indicates the presence of the surface Cu²⁺ species in copper compounds and CuCrS₂-based solid solutions [33,35,36,48]. The sharp symmetric line-shape observed in the measured Cu2p-lines additionally confirms the absence of the surface Cu²⁺ species. However, the reported data concerning the copper oxidation state in the initial CuCrS₂-matrix also indicated the absence of the Cu²⁺ state in CuCrS₂ synthesized using pure elements and metal-organic reagents [1,21,40]. A systematic study of the charge distribution in CuCrS₂-based solid solutions using both the surface-sensitive XPS technique and bulk-sensitive techniques (X-ray spectroscopy and magnetochemistry) showed that Cu²⁺ was localized on the surface [32,33,35,36,39,49]. Thus, varying the synthesis route allows one to obtain samples with or without Cu²⁺ on the sample surface. The measured BE values of the main Cu2p_{3/2}-line were in the range of 931.6 to 932.0 eV and correspond to Cu⁺ in sulfide and selenide compounds of copper (Cu₂S, BE ≈ 932.0 ÷ 932.2 eV; Cu₂Se, BE ≈ 931.0 ÷ 932.2 eV [50,51]). The lanthanum concentration increase did not significantly affect the BE of Cu2p_{3/2}-lines in CuCr_{1-x}La_xS₂ solid solutions. Thus, one can conclude that the cationic substitution in CuCr_{1-x}La_xS₂ did not significantly affect the electronic density localized on the copper atoms. The measured BE of Cu2p_{3/2}-lines in CuLaS₂ was in the same energy range as that for CuCr_{1-x}La_xS₂. This fact indicates that CuLaS₂ impurity phase did not significantly affect the Cu2p-region in CuCr_{1-x}La_xS₂. Note that the Cu2p_{3/2} BE values measured in the present study were shifted to the low-energy region compared to those for CuCrS₂-based solid solutions obtained from the metal oxide initial reagents reported previously (CuCrS₂, CuCr_{1-x}M_xS₂, BE ≈ 932.2 ÷ 932.6 eV) [33,36]. This could be due to the significant covalence contribution of the M-S bonding compared to the M-O. For instance, the M-S bonding leads to greater localization of the electron density on copper atoms in the sulfides compared to oxide compounds [52]. Note that the BE values of Cu2p_{3/2}-lines for CuCrS₂ samples obtained using pure elements or metal-organic compounds were within the range of 932.0 to 932.1 eV [1,21,40]. Thus, one can conclude that the BE of Cu2p-lines could vary depending on the synthesis route.

The Cr2p-region for CuCr_{1-x}La_xS₂ is depicted in Figure 3a. The spin-orbit doublet of Cr2p_{1/2}- and Cr2p_{3/2}-lines can be observed, similar to the case of Cu2p-lines. However, the line-shape of the Cr2p-lines is asymmetric with a shoulder in the high-energy region. Thus, one can conclude that the Cr2p-region represents a superposition of two components. The low-energy line (marked as I in Figure 3a) with a BE of 574.2 to 574.5 eV could be associated with the Cr³⁺ in sulfide (Cr₂S₃ BE ≈ 574.4–575.4 eV) or selenide (Cr₂Se₃ BE ≈ 574.4–575.4 eV, CuCrSe₂, BE ≈ 574.7 eV; CuCr₂Se₄, BE ≈ 574.5 eV) compounds of chromium [40,50,51]. As it was previously reported in [33,36], the high-energy line (marked as II in Figure 3a) with a BE of 576.6 to 577.2 eV is attributed to the oxide compounds of chromium on the sample surface (Cr₂O₃, BE ≈ 576.5 eV; CuCrO₂, BE ≈ 576.0 eV [50,51]). Hence, the low-energy components are considered to correspond to the chromium atoms in CuCr_{1-x}La_xS₂ solid solutions. Thus, one can conclude that cationic substitution did not affect the BE of the Cr2p lines and, thereby, the electron density localized on the chromium atoms. Note that measured BE values were shifted to the low-energy region compared to those for CuCrS₂-based solid solutions obtained from the metal oxide initial reagents reported previously (BE ≈ 574.6–574.8 [33,36]). In the case of CuCrS₂ obtained using pure elements, the BE of the Cr2p_{3/2}-line was within the range of 574.6 to 574.8 eV [1,40]. Of particular note is that in the case of CuCrS₂ synthesized using metal-organic reagents, the BE of 576.6 eV, corresponding to the Cr2p_{3/2}-line, was significantly shifted to the high-energy region [21]. The observed shift could indicate a significant oxidation of chromium atoms in the near-surface layers of the sample. However, the contribution of the II component prevailed. Thus, one can conclude that the Cr2p-region, as well as the Cu2p-region, was significantly affected by the synthesis route. Note that the integral inten-

sity ratio of the components in the Cr2p-region of $\text{CuCr}_{1-x}\text{La}_x\text{S}_2$ was more variable than it was observed previously for $\text{CuCr}_{0.99}\text{Ln}_{0.01}\text{S}_2$ ($\text{Ln} = \text{La} \dots \text{Lu}$) solid solutions synthesized using metal oxide reagents [33,35,36]. The most intense component II was observed for $\text{CuCr}_{0.97}\text{Ln}_{0.03}\text{S}_2$ solid solution. This could be due to the highest concentration of CuLaS_2 impurity phase, which results in increased defectiveness of the chromium sublattice and, consequently, the lighter oxidation of chromium atoms in the near-surface layers.

The S2p-region for $\text{CuCr}_{1-x}\text{La}_x\text{S}_2$ is represented by an unresolved line consisting of the $\text{S}2\text{p}_{1/2}$ - and $\text{S}2\text{p}_{3/2}$ -components of the spin-orbit doublet (Figure 2b). Note that the S2p-region exhibits two groups of lines. The first group of lines (denoted as I in Figure 2b) with a BE of 160.6–161.0 eV arises from the sulfur atoms in the composition of $\text{CuCr}_{1-x}\text{La}_x\text{S}_2$ and corresponds to the S^{2-} state [33,36,50]. Thus, taking into account the measured BE values of the corresponding components, one can conclude that cationic substitution of the initial CuCrS_2 -matrix did not affect electron density localized on the sulfur atoms. The measured BE values correlate with those for transition metal sulfides (FeS , BE \approx 160.8–161.4 eV; TiS_2 , BE \approx 160.9 eV; CuFeS_2 , BE \approx 161.5 eV [50,51]). The second group (denoted as II in Figure 2b) with a BE of 162.5–162.7 eV is associated with the sulfur atoms of polysulfide groups and elemental sulfur in the defective near-surface layers on the samples. Note that the presence of the corresponding sulfur surface species is typical for inorganic sulfur compounds [53,54]. The measured S2p-lines for $\text{CuCr}_{1-x}\text{La}_x\text{S}_2$ were shifted to the low-energy region compared to the samples synthesized using the metal oxide reagents (BE \approx 160.9–161.5 eV [33,36,50]). Meanwhile, CuCrS_2 samples synthesized using meta-organic reagents exhibited an intermediate S2p-line BE of 161.0 eV [21]. The S2p-region for the impurity CuLaS_2 phase is represented with the same line-shape as the solid solutions studied (Figure 2b). The measured BE for CuLaS_2 was slightly shifted in the low-energy spectral region. This fact allows one to conclude that the presence of the impurity CuLaS_2 phase in the composition of the final $\text{CuCr}_{1-x}\text{La}_x\text{S}_2$ products could lead to a slight shift of the S2p-line to the low-energy region if the CuLaS_2 concentration is high.

The La3d-region for $\text{CuCr}_{1-x}\text{La}_x\text{S}_2$ solid solutions is presented in Figure 3b. Note that the spin-orbit splitting value for the La3d-level is \sim 17 eV. Thus, the $\text{La}3\text{d}_{5/2}$ -line could be analyzed separately from $\text{La}3\text{d}_{3/2}$. The $\text{La}3\text{d}_{5/2}$ -line exhibits two intense components (denoted as 1 and 2) arising due to the many-electron process [47]. The main low-energy line with a BE of 834.7–834.9 eV correlates well with the La^{3+} oxidation state (La_2O_3 , BE \approx 834.0–835.2 eV [50,51]). The absence of significant shifts of the La3d-line indicated the preservation of electron density localized on the lanthanum atoms in $\text{CuCr}_{1-x}\text{La}_x\text{S}_2$ with an increase in lanthanum concentration. However, the line-shape for $\text{CuCr}_{1-x}\text{La}_x\text{S}_2$ ($x > 0.01$) solid solutions changed. This resulted in the evolution of the line-shape, and for $x = 0.03$, the $\text{La}3\text{d}_{5/2}$ -line was similar to that for CuLaS_2 and corresponded to the impurity phase concentration increase. Taking into account the relatively low total lanthanum concentration in comparison to other elements in $\text{CuCr}_{1-x}\text{La}_x\text{S}_2$, CuLaS_2 could noticeably impact the line-shape even when the impurity phase concentration was low. The measured BE of $\text{La}3\text{d}_{5/2}$ -lines was shifted to the low-energy region compared to the previously investigated samples synthesized using the metal oxide reagents ($\text{CuCr}_{0.99}\text{La}_{0.01}\text{S}_2$, BE \approx 835.4 eV [35]).

Static magnetic measurements can provide data concerning the effective magnetic moment, the magnetic phase transition temperature, the presence of specific *magnetic* impurities, and the exchange interactions between the magnetic centers in the sample studied. Since the μ_{eff} of transition elements depends on their oxidation state, one could obtain data concerning the electronic density localized on the magnetic centers. However, in the case of complex chemical compounds containing a few different types of magnetic centers, the interpretation of μ_{eff} values could be significantly complicated due to the macroscopic behavior of the method [55,56]. Magnetochemistry data are used as a method to study charge distribution in CuCrS_2 -based solid solutions [10,11,14,34,38,39,42,57]. Note that the obtained data led to contradictory conclusions regarding the oxidation state of copper and chromium ions, even in the initial CuCuS_2 -matrix. For instance, studies have shown Cu^+ and Cr^{2+} [9], the coexistence of $\text{Cu}^+/\text{Cr}^{3+}$ and $\text{Cu}^{2+}/\text{Cr}^{2+}$ distributions [14,58], and Cu^+ and Cr^{3+} [57]. The

systematic studies involving both the macroscopic static magnetochemistry measurements and element-selective XPS and X-ray spectroscopy techniques allow one to conclude that deviations from the simple charge balance model of $\text{Cu}^+\text{Cr}^{3+}(\text{S}^{2-})_2$ could be attributed to the presence of magnetic impurities and surface oxidation state species [32–36,39]. However, the reported data could be attributed to the sample series obtained by using the same synthesis route using metal oxide initial reagents. Here, we report a study of magnetic properties for the samples synthesized using metal sulfide initial reagents and attempt to assess the potential influence of the synthesis route on the obtained data.

The magnetic properties of $\text{CuCr}_{1-x}\text{La}_x\text{S}_2$ solid solutions synthesized using the metal sulfide initial reagents are presented in Figure 4. It was previously reported that the inverse magnetic susceptibility ($1/\chi$) of similar samples synthesized using metal oxide initial reagents showed a linear dependence on temperature within the temperature range of 80 to 600 K [42]. However, the solid solutions $\text{CuCr}_{0.995}\text{La}_{0.005}\text{S}_2$ and $\text{CuCr}_{0.985}\text{La}_{0.015}\text{S}_2$ demonstrated deviations from linear dependence. The observed deviation consequently affected the behavior of the $\chi(T)$ and $\mu_{\text{eff}}(T)$ dependencies compared to the other samples. The most significant deviation was observed at temperatures below 400 K. The presence of magnetic impurities leads to the overestimation of μ_{eff} [55]. The positive slope of χ as the function of the inverse value of the applied magnetic field strength for $\text{CuCr}_{0.995}\text{La}_{0.005}\text{S}_2$ and $\text{CuCr}_{0.985}\text{La}_{0.015}\text{S}_2$ indicated the influence of ferromagnetic impurities at $T < 400$ K (as shown in the inset in Figure 4a) [55]. The behavior of $\chi(T)$, $1/\chi(T)$, and $\mu_{\text{eff}}(T)$ dependencies (marked as 0.005* and 0.015* in Figure 4) was similar to that for the other samples after the correction procedure. The corrected and non-corrected data correlate well at $T > 400$ K. Note that other samples did not contain ferromagnetic impurities. The magnetic susceptibility of the impurity CuLaS_2 phase was negative. This fact indicated that CuLaS_2 is diamagnetic. The absolute value of χ for CuLaS_2 was two orders of magnitude lower compared to the main $\text{CuCr}_{1-x}\text{La}_x\text{S}_2$ phase. Thus, one can conclude that the presence of the diamagnetic impurity did not significantly affect the magnetic properties of the main phase. That fact correlates well with the previously reported data [42].

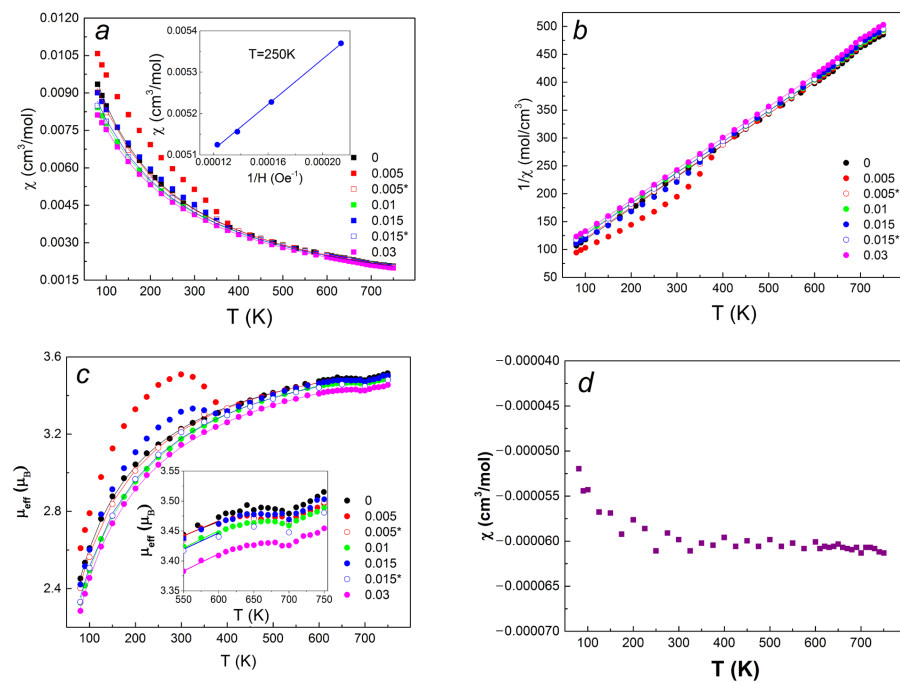


Figure 4. Temperature dependencies of magnetic susceptibility (a,d), inverse magnetic susceptibility (b), and effective magnetic moment (c,d) for $\text{CuCr}_{1-x}\text{La}_x\text{S}_2$ (a–c) solid solutions and CuLaS_2 (d). *—data after correction procedure.

A slight decrease in the χ and μ_{eff} values is observed (Figure 4a and inset in Figure 4c, respectively) within the temperature range of 600–750 K. It was previously reported that the observed behavior is associated with the order-disorder phase transition (ODT) [34,42]. Hence, one can conclude that the data on magnetic properties can provide additional information on the order-disorder phase transition temperature for the samples studied. The concentration dependency of the μ_{eff} minimum temperature for $\text{CuCr}_{1-x}\text{La}_x\text{S}_2$ is shown in Figure 5. A general trend of the μ_{eff} minimum temperature decreasing as a function of lanthanum concentration is observed. It was previously suggested that the observed behavior could be associated with a decrease in the defect formation energy [42]. Thus, the dependencies of the μ_{eff} minimum temperature for the samples synthesized from metal sulfide reagents correlate with those reported for the samples obtained using metal oxide reagents.

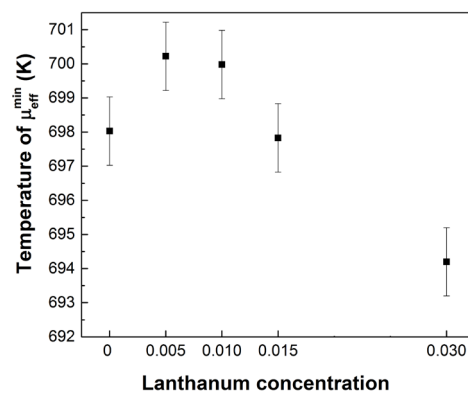


Figure 5. Minimum temperature of effective magnetic moment for $\text{CuCr}_{1-x}\text{La}_x\text{S}_2$ solid solutions.

The temperature dependencies of χ after the correction procedure were approximated according to the Curie–Weiss law (solid lines in Figure 4) [55]. The concentration dependencies of the μ_{eff} and Weiss constant (Θ) are presented in Figures 6a and 6b, respectively. The μ_{eff} value of $3.77 \mu_{\text{B}}$ measured for the initial CuCrS_2 -matrix correlates well with the experimental values of the μ_{eff} for Cr^{3+} compounds. However, the obtained value is slightly less than the theoretical value of $3.87 \mu_{\text{B}}$ [55,56]. The obtained value is less compared to the sample synthesized using metal oxide reagents [42]. Note that the concentration dependency of the μ_{eff} for $\text{CuCr}_{1-x}\text{La}_x\text{S}_2$ shown in Figure 6 deviates from that reported in [42]. The μ_{eff} increased for $\text{CuCr}_{1-x}\text{La}_x\text{S}_2$ ($x \leq 0.01$), while in the case of samples obtained using metal oxide reagents, it decreased. This fact contradicts the simple model of the cationic substitution of paramagnetic Cr^{3+} with diamagnetic La^{3+} ions, which assumes a μ_{eff} decrease. Note that the oxidation states of metal atoms determined using XPS were Cu^+ , Cr^{3+} , and La^{3+} . Thus, only the Cr^{3+} ions carry the magnetic moment due to the presence of unpaired electrons on the 3d-shell. Hence, the slight variation of the μ_{eff} value is attributed to the fluctuation of the electronic density localized on chromium atoms. This could be due to the sample defectiveness resulting from the incorporation of La^{3+} ions during the cationic substitution, as suggested in previous studies [42]. The μ_{eff} value decrease for $x > 0.01$ could be related to the diamagnetic impurity CuLaS_2 phase formation [42]. The concentration dependencies of the Weiss constant Θ can be represented by two characteristic ranges of $x \leq 0.01$ and $x > 0.01$, respectively. The first one corresponds to a notable decrease in the absolute value of Θ , and the second one is associated with minor variations in the absolute value of Θ . In terms of the molecular field theory, the Θ value is associated with the spin localized on the magnetic center and the absolute value of the total magnetic exchange interaction $|\sum_i z_i|$ [55,56]. Since the La^{3+} ions are diamagnetic, the $|\sum_i z_i|$ could be simply calculated (Figure 6c) as was described in [39,42]. The $|\sum_i z_i|$ value increased for $\text{CuCr}_{1-x}\text{La}_x\text{S}_2$ ($x \leq 0.01$). This could be due to the increase in electronic density localized on the chromium atoms and, consequently, the overlap of the electron cloud of the chromium atoms with

the electron densities of the neighboring atoms. The second concentration range $x > 0.01$ corresponds to the formation of the impurity CuLaS_2 phase.

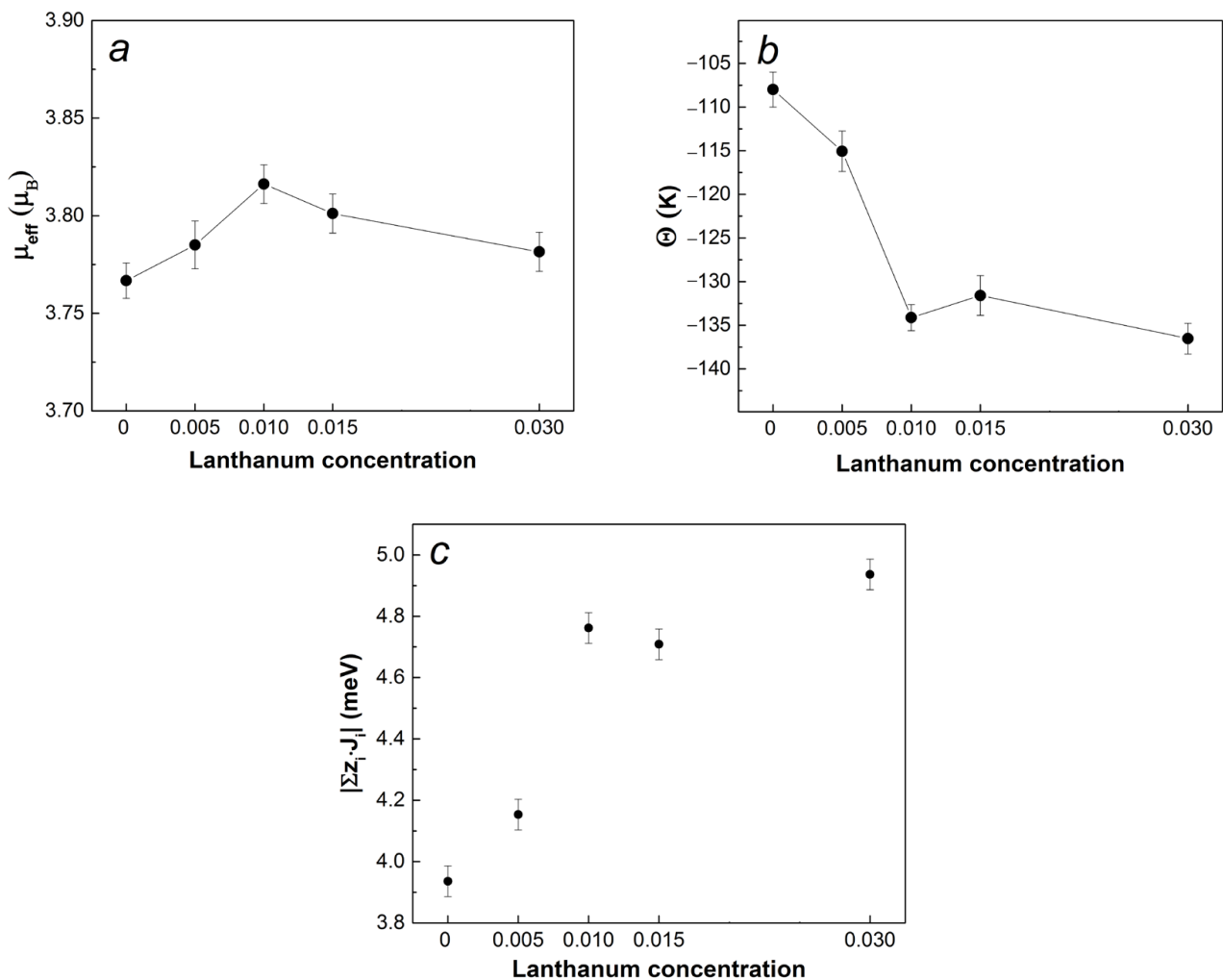


Figure 6. Concentration dependencies of effective magnetic moment (a), Weiss constants (b), and total magnetic exchange interaction absolute value (c) for $\text{CuCr}_{1-x}\text{La}_x\text{S}_2$ solid solutions.

In addition to the data on the atom oxidation state, XPS spectroscopy allows one to obtain experimental data concerning the valence band (VB) structure [47]. The VB structure and the partial density of states (DOS) for the initial CuCrS_2 -matrix and $\text{CuCr}_{0.99}\text{La}_{0.01}\text{S}_2$ solid solutions obtained using oxygen metal initial reagents were discussed previously [3,35]. An example of the theoretical VB calculation based on the DOS calculations for the initial CuCrS_2 -matrix is presented in Figure 7a. It was previously demonstrated that the simple broadening of the total density of states (denoted “DOS” in Figure 7a) using the $\text{AlK}\alpha$ -line width (“DOS br.” in Figure 7a) did not yield a good agreement between the theoretical and experimental data [35]. Taking into account the photoionization cross-section value (σ_{ph}), one could recalculate the partial contribution in the total DOS (“DOS $\times \sigma_{\text{ph}}$ ” in Figure 7a) and broaden it using the $\text{AlK}\alpha$ -line width (“DOS $\times \sigma_{\text{ph}}$ br.” in Figure 7a). The line-shape of the calculated VB correlates well with the experimental VB. Since the copper atoms have a higher σ_{ph} value, the experimental VB is mainly determined by the copper states, resulting in a triangle-like line-shape. For the calculation of the lanthanide-doped $\text{CuCr}_{1-x}\text{La}_x\text{S}_2$, the variation in lanthanum concentration was taken into account by a simple recalculation of the partial contribution of the lanthanum DOS reported previously [35]. The theoretical VB spectra for $\text{CuCr}_{1-x}\text{La}_x\text{S}_2$ ($x = 0.005\text{--}0.03$) solid solutions are presented in Figure 7b. The similarity of the line-shape of both theoretical and experimental VB (Figure 7c) allows one to

conclude that cationic substitution did not significantly affect the partial DOS distribution in the VB of $\text{CuCr}_{1-x}\text{La}_x\text{S}_2$. This could be due to the low lanthanum concentration and, therein, low contributions of the lanthanum states in the VB structure. Furthermore, the lanthanum has an unfilled 4f-shell. Thus, the contribution of the lanthanum states is low, especially when compared to the contribution of the copper states. The experimental VB of the impurity CuLaS_2 phase has a similar shape to the one for $\text{CuCr}_{1-x}\text{La}_x\text{S}_2$ solid solutions (Figure 7c). Thus, one can conclude that the presence of CuLaS_2 impurity in the composition of $\text{CuCr}_{1-x}\text{La}_x\text{S}_2$ samples did not significantly distort the VB structure.

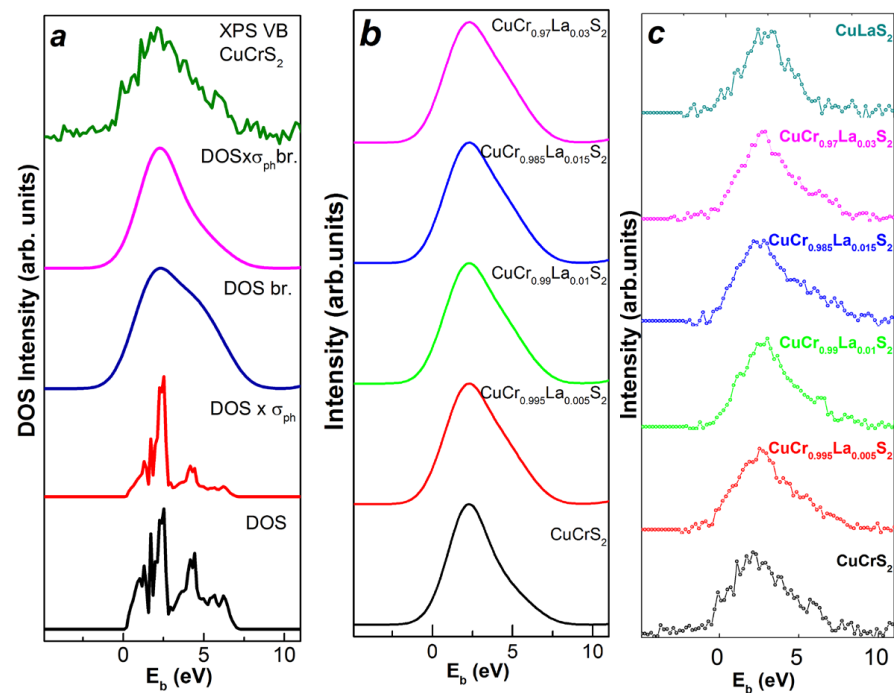


Figure 7. Density of states distribution (a), theoretical valence band spectra (b), and experimental XPS valence band spectra (c) of $\text{CuCr}_{1-x}\text{La}_x\text{S}_2$ solid solutions.

The Seebeck coefficient (S) temperature dependencies for $\text{CuCr}_{1-x}\text{La}_x\text{S}_2$ solid solutions studied are plotted in Figure 8a. The S values measured in the current study are higher compared to the previously reported data for the samples obtained using metal oxide initial reagents [42]. Thus, the Seebeck coefficient of CuCrS_2 -based solid solutions could be increased by changing the synthesis route. In the case of initial metal oxide reagents, during the sulfidation procedure, the oxygen atoms in the reaction mixture are replaced by the sulfur atoms from the sulfidation atmosphere. When one uses sulfide metal initial reagents, the sulfidation atmosphere prevents sulfur depletion from the reaction mixture. Hence, in the first route, some residual oxygen could be preserved after the sulfidation procedure in the composition of samples. The residual oxygen atoms could introduce additional dopant or trap centers, affecting the total charge carrier concentration and S values. Note that the sample defectiveness increase discussed above could also impact the total carrier concentration. The Seebeck coefficient of $\text{CuCr}_{1-x}\text{La}_x\text{S}_2$ tended to saturate at high temperatures ($T > 400$ K). It should be noted that using the metal oxides as the initial reagents resulted in a shift of the saturation to a higher temperature region ($T > 500$ K) [42] due to the presence of the residual oxygen affecting the total carrier concentration [45]. The charge carrier concentration measured at room temperature is plotted in Figure 7b. The carrier concentration (holes according to the Hall voltage polarity) measured for the initial CuCrS_2 -matrix ($1.5 \cdot 10^{17}$) is lower compared to that previously reported for the samples obtained using metal oxygen reagents ($6.8 \cdot 10^{17}$) [42].

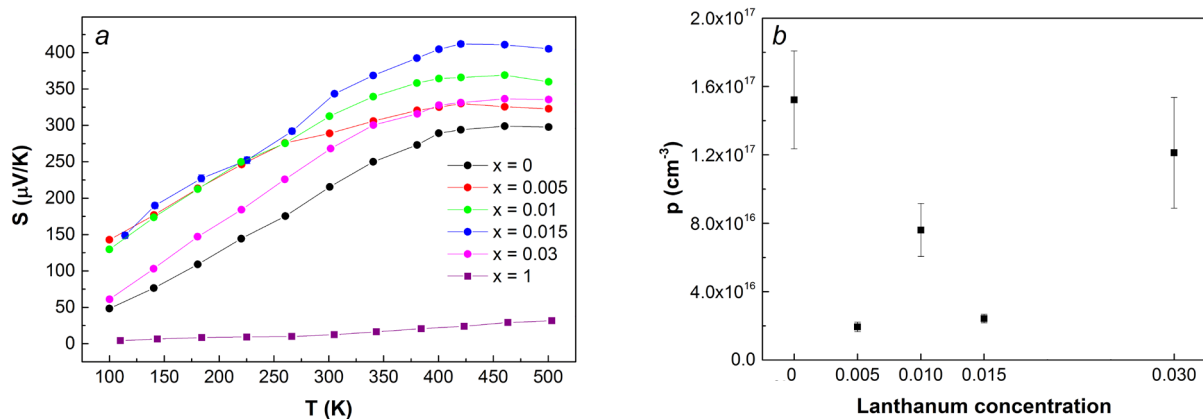


Figure 8. Seebeck coefficient temperature dependence (a) and carrier concentration at room temperature (b) for $\text{CuCr}_{1-x}\text{La}_x\text{S}_2$ solid solutions.

As was reported previously [32,33,35,36,42], the cationic substitution of chromium atoms in CuCrS_2 -matrix with lanthanum atoms leads to an increase in the S value, as observed in Figure 8. The maximum S value of $412 \mu\text{V}/\text{K}$ was measured for $\text{CuCr}_{0.985}\text{La}_{0.015}\text{S}_2$ at 420 K. The obtained value is higher compared to the maximum value of $373 \mu\text{V}/\text{K}$ reported in [42]. Further increasing the lanthanum concentration to $x = 0.03$ caused a suppression of the Seebeck coefficient. The observed concentration behavior of the Seebeck coefficient correlated with electronic structure reconfiguration reported for lanthanum-doped and CuCrS_2 -based solid solutions [3,32,33,35,36,42]. For instance, at low concentrations $x \leq 0.015$, the S value of $\text{CuCr}_{1-x}\text{La}_x\text{S}_2$ increases due to the shift of the valence band top to a higher binding energy region. The further concentration increase gradually leads to the band gap narrowing, ultimately resulting in it completely vanishing at high dopant concentrations [3,34]. The corresponding model is in good agreement with the measured carrier concentrations presented in Figure 8b. The carrier concentration decreasing at $x = 0.005$ could be related to the shift of the valence band top. The carrier concentration increased at $x \geq 0.01$ due to the band gap narrowing. The deviation of the carrier concentration from the increasing trend at $x = 0.015$ could be attributed to the presence of the CuLaS_2 impurity. Thus, the synthesis route could affect both the Seebeck coefficient value and carrier concentration. The variation of the initial reagents from the metal oxides to sulfides initial reagents could be utilized to increase the Seebeck coefficient.

4. Conclusions

A comprehensive study involving XPS spectroscopy, static magnetochemistry, the Seebeck coefficient, and the Hall voltage measurements for the lanthanum-substituted solid solutions $\text{CuCr}_{1-x}\text{La}_x\text{S}_2$ ($x = 0, 0.005, 0.01, 0.015, \text{ and } 0.03$) synthesized using metal sulfide initial reagents was carried out. It was shown that the cationic substitution occurs via the isovalent principle $\text{Cr}^{3+} \rightarrow \text{La}^{3+}$ for all lanthanum concentrations. The cationic substitution did not affect the charge distribution on the matrix elements Cu^+ , Cr^{3+} , and S^{2-} . The most significant effect of the impurity CuLaS_2 phase was observed in the Ln3d-region. The measured BE of Cu2p-, Cr2p-, S2p- and La3d-lines were shifted to the low-energy region compared to the previously reported data for the CuCrS_2 -based solid solutions obtained using the metal oxide initial reagents. This could be due to the significant covalence contribution of the M-S bonding compared to the M-O. The magnetic properties of $\text{CuCr}_{1-x}\text{La}_x\text{S}_2$ solid solutions synthesized using metal sulfide reagents cannot be interpreted using the simple isovalent Cr^{3+} to La^{3+} cationic substitution model. The defectiveness of the samples and the formation of the impurity CuLaS_2 phase could be additional factors that affect the magnetic properties of $\text{CuCr}_{1-x}\text{La}_x\text{S}_2$ solid solutions. The concentration dependencies of the μ_{eff} , Θ , and $|\sum_j z_j|$ were significantly influenced by the synthesis route. The cationic substitution did not significantly affect the partial density of states distribution in the ex-

perimental valence band structure of $\text{CuCr}_{1-x}\text{La}_x\text{S}_2$ solid solutions. The maximum Seebeck coefficient value of $412 \mu\text{V}/\text{K}$ was measured for $\text{CuCr}_{0.985}\text{La}_{0.015}\text{S}_2$ at 420 K. An increase in the lanthanum concentration to $x = 0.03$ caused a suppression of the Seebeck coefficient. The variation of the initial reagents from the metal oxides to sulfides initial reagents can be utilized to increase the Seebeck coefficient.

Author Contributions: Conceptualization, E.V.K. and M.M.S.; Methodology, E.V.K., M.M.S. and I.Y.F.; Validation, E.V.K.; Formal analysis, M.M.S.; Investigation, E.V.K. and M.M.S.; Resources, I.Y.F. and E.V.K.; Data curation, E.V.K. and M.M.S.; Writing—original draft, E.V.K. and M.M.S.; Writing—review and editing, E.V.K. and M.M.S.; Visualization, E.V.K. and M.M.S.; Supervision, E.V.K.; Funding acquisition, E.V.K. All authors have read and agreed to the published version of the manuscript.

Funding: This study was funded by the Russian Science Foundation (project No. 19-73-10073, <https://rscf.ru/project/19-73-10073/> accessed 14 November 2022).

Institutional Review Board Statement: Not applicable.

Informed Consent Statement: Not applicable.

Data Availability Statement: Not applicable.

Acknowledgments: The authors are grateful to the Ministry of Science and Higher Education of the Russian Federation. The authors thank Sotnikov A.V. for the assistance with obtaining the ceramic samples.

Conflicts of Interest: The authors declare no conflict of interest.

References

1. Tewari, G.C.; Tripathi, T.S.; Rastogi, A.K. Thermoelectric properties of layer-antiferromagnet CuCrS_2 . *J. Electron. Mater.* **2010**, *39*, 1133–1139. [[CrossRef](#)]
2. Tewari, G.C.; Tripathi, T.S.; Rastogi, A.K. Effect of chromium disorder on the thermoelectric properties of layered-antiferromagnet CuCrS_2 . *Z. Für Krist.* **2010**, *225*, 471–474. [[CrossRef](#)]
3. Korotaev, E.V.; Syrovkashin, M.M.; Filatova, I.Y.; Pelmenov, K.G.; Zvereva, V.V.; Peregodova, N.N. Seebeck Coefficient of Cation-Substituted Disulfides $\text{CuCr}_{1-x}\text{FexS}_2$ and $\text{Cu}_{1-x}\text{FexCrS}_2$. *J. Electron. Mater.* **2018**, *47*, 3392–3397. [[CrossRef](#)]
4. Kaltzoglou, A.; Vaqueiro, P.; Barbier, T.; Guilmeau, E.; Powell, A.V. Ordered-Defect Sulfides as Thermoelectric Materials. *J. Electron. Mater.* **2014**, *43*, 2029–2034. [[CrossRef](#)]
5. Romanenko, A.I.; Chebanova, G.E.; Katamanin, I.N.; Drozhzhin, M.V.; Artemkina, S.B.; Han, M.-K.; Kim, S.-J.; Wang, H. Enhanced thermoelectric properties of polycrystalline $\text{CuCrS}_2-x\text{Sex}$ ($x = 0, 0.5, 1.0, 1.5, 2$) samples by replacing chalcogens and sintering. *J. Phys. D Appl. Phys.* **2021**, *55*, 135302. [[CrossRef](#)]
6. Hansen, A.-L.; Dankwort, T.; Groß, H.; Etter, M.; König, J.; Duppel, V.; Kienle, L.; Bensch, W. Structural properties of the thermoelectric material CuCrS_2 and of deintercalated Cu_xCrS_2 on different length scales: X-ray diffraction, pair distribution function and transmission electron microscopy studies. *J. Mater. Chem. C* **2017**, *5*, 9331–9338. [[CrossRef](#)]
7. Chen, Y.-X.; Zhang, B.-P.; Ge, Z.-H.; Shang, P.-P. Preparation and thermoelectric properties of ternary superionic conductor CuCrS_2 . *J. Solid. State Chem.* **2012**, *186*, 109–115. [[CrossRef](#)]
8. Krengel, M.; Hansen, A.L.; Hartmann, F.; van Dinter, J.; Bensch, W. Elucidation of the Sodium—Copper Extrusion Mechanism in CuCrS_2 : A High Capacity, Long-Life Anode Material for Sodium-Ion Batteries. *Batter. Supercaps* **2018**, *1*, 176–183. [[CrossRef](#)]
9. Almukhametov, R.F.; Yakshibayev, R.A.; Gabitov, E.V.; Abdullin, A.R.; Kutusheva, R.M. Structural properties and ionic conductivities of $\text{CuCr}_{1-x}\text{V}_x\text{S}_2$ solid solutions. *Phys. Status Solidi* **2003**, *236*, 29–33. [[CrossRef](#)]
10. Almukhametov, R. Structural properties and ionic conductivity of new $\text{CuCr}_{1-x}\text{V}_x\text{Se}_2$ solid solutions. *Solid. State Ion.* **2003**, *158*, 409–414. [[CrossRef](#)]
11. Vasilyeva, I.G. Chemical aspect of the structural disorder in CuCrS_2 and $\text{CuCr}_{1-x}\text{V}_x\text{S}_2$ solid solutions. *J. Struct. Chem.* **2017**, *58*, 1009–1017. [[CrossRef](#)]
12. Vassilieva, I.G.; Kardash, T.Y.; Malakhov, V.V. Phase transformations of CuCrS_2 : Structural and chemical study. *J. Struct. Chem.* **2009**, *50*, 288–295. [[CrossRef](#)]
13. Peng, J.; Chen, Z.-J.; Ding, B.; Cheng, H.-M. Recent Advances for the Synthesis and Applications of 2-Dimensional Ternary Layered Materials. *Research* **2023**, *6*, 40. [[CrossRef](#)] [[PubMed](#)]
14. Abramova, G.M.; Petrakovskii, G.A. Metal-insulator transition, magnetoresistance, and magnetic properties of 3d-sulfides (Review). *Low. Temp. Phys.* **2006**, *32*, 725–734. [[CrossRef](#)]
15. Rasch, J.C.E.; Boehm, M.; Ritter, C.; Mutka, H.; Schefer, J.; Keller, L.; Abramova, G.M.; Cervellino, A.; Löffler, J.F. Magnetoelastic coupling in the triangular lattice antiferromagnet CuCrS_2 . *Phys. Rev. B* **2009**, *80*, 104431. [[CrossRef](#)]

16. Tsujii, N.; Kitazawa, H.; Kido, G. Insulator to metal transition induced by substitution in the nearly two-dimensional compound $\text{CuCr}_{1-x}\text{V}_x\text{S}_2$. *Phys. Status Solidi* **2006**, *3*, 2775–2778. [[CrossRef](#)]
17. Engelsman, F.M.R.; Wieggers, G.A.; Jellinek, F.; Van Laar, B. Crystal structures and magnetic structures of some metal (I) chromium (III) sulfides and selenides. *J. Solid. State Chem.* **1973**, *6*, 574–582. [[CrossRef](#)]
18. Karmakar, A.; Dey, K.; Chatterjee, S.; Majumdar, S.; Giri, S. Spin correlated dielectric memory and rejuvenation in multiferroic CuCrS_2 . *Appl. Phys. Lett.* **2014**, *104*, 052906. [[CrossRef](#)]
19. Winterberger, M.; Allain, Y.; Winterberger, M.A.Y. Structure magnetique helicoidale de CuCrS_2 . *Solid. State Commun.* **1987**, *64*, 1343–1346. [[CrossRef](#)]
20. Sanchez Rodriguez, J.J.; Nunez Leon, A.N.; Abbasi, J.; Shinde, P.S.; Fedin, I.; Gupta, A. Colloidal Synthesis, Characterization, and Photoconductivity of Quasi-Layered CuCrS_2 Nanosheets. *Nanomaterials* **2022**, *12*, 4164. [[CrossRef](#)]
21. Lee, H.K.; Ban, Y.J.; Lee, H.J.; Kim, J.H.; Park, S.J. One-Pot Synthesis and Characterization of $\text{CuCrS}_2/\text{ZnS}$ Core/Shell Quantum Dots as New Blue-Emitting Sources. *Materials* **2023**, *16*, 762. [[CrossRef](#)]
22. Xu, X.; Zhong, T.; Zuo, N.; Li, Z.; Li, D.; Pi, L.; Chen, P.; Wu, M.; Zhai, T.; Zhou, X. High-Temperature Two-Dimensional Ferroelectric CuCrS_2 Grown via Chemical Vapor Deposition. *ACS Nano* **2022**, *16*, 8141–8149. [[CrossRef](#)] [[PubMed](#)]
23. Zhong, T.; Li, X.; Wu, M.; Liu, J.M. Room-temperature multiferroicity and diversified magnetoelectric couplings in 2D materials. *Natl. Sci. Rev.* **2020**, *7*, 373–380. [[CrossRef](#)] [[PubMed](#)]
24. Kousar, H.S.; Srivastava, D.; Karppinen, M.; Tewari, G.C. Tunable Low-Temperature Thermoelectric Transport Properties in Layered $\text{CuCr}(\text{S}_{1-x}\text{Se}_x)_2$ System. *Z. Fur Anorg. Und Allg. Chem.* **2023**, *649*, e202300079. [[CrossRef](#)]
25. Wu, D.; Huang, S.; Feng, D.; Li, B.; Chen, Y.; Zhang, J.; He, J. Revisiting AgCrSe_2 as a promising thermoelectric material. *Phys. Chem. Chem. Phys.* **2016**, *18*, 23872–23878. [[CrossRef](#)] [[PubMed](#)]
26. Yin, Y.; Baskaran, K.; Tiwari, A. A Review of Strategies for Developing Promising Thermoelectric Materials by Controlling Thermal Conduction. *Phys. Status Solidi Appl. Mater. Sci.* **2019**, *216*, 6–8. [[CrossRef](#)]
27. Zebarjadi, M.; Esfarjani, K.; Dresselhaus, M.S.; Ren, Z.F.; Chen, G. Perspectives on thermoelectrics: From fundamentals to device applications. *Energy Environ. Sci.* **2012**, *5*, 5147–5162. [[CrossRef](#)]
28. Tan, X.; Ding, J.; Luo, H.; Delaire, O.; Yang, J.; Zhou, Z.; Lan, J.L.; Lin, Y.H.; Nan, C.W. High Thermoelectric Performance of $\text{AgSb}_{1-x}\text{Pb}_x\text{Se}_2$ Prepared by Fast Nonequilibrium Synthesis. *ACS Appl. Mater. Interfaces* **2020**, *12*, 41333–41341. [[CrossRef](#)] [[PubMed](#)]
29. Wang, J.; Yan, X.; Zhang, Z.; Guo, R.; Ying, H.; Han, G.; Han, W.-Q. Rational Design of an Electron/Ion Dual-Conductive Cathode Framework for High-Performance All-Solid-State Lithium Batteries. *ACS Appl. Mater. Interfaces* **2020**, *12*, 41323–41332. [[CrossRef](#)]
30. Li, S.; Hou, S.; Xue, W.; Yin, L.; Liu, Y.; Wang, X.; Chen, C.; Mao, J.; Zhang, Q. Manipulation of phase structure and Se vacancy to enhance the average thermoelectric performance of AgBiSe_2 . *Mater. Today Phys.* **2022**, *27*, 100837. [[CrossRef](#)]
31. Wu, H.; Shi, X.; Duan, J.; Liu, Q.; Chen, Z.-G. Advances in Ag₂Se-based thermoelectrics from materials to applications. *Energy Environ. Sci.* **2023**, *16*, 1870–1906. [[CrossRef](#)]
32. Korotaev, E.V.; Syrokvashin, M.M.; Filatova, I.Y.; Trubina, S.V.; Nikolenko, A.D.; Ivlyushkin, D.V.; Zavertkin, P.S.; Sotnikov, A.V.; Kriventsov, V.V. XANES investigation of novel lanthanide-doped $\text{CuCr}_{0.99}\text{Ln}_{0.01}\text{S}_2$ ($\text{Ln} = \text{La}, \text{Ce}$) solid solutions. *Appl. Phys. A* **2020**, *126*, 537. [[CrossRef](#)]
33. Korotaev, E.V.; Syrokvashin, M.M.; Filatova, I.Y.; Sotnikov, A.V.; Kalinkin, A. V The Charge Distribution, Seebeck Coefficient, and Carrier Concentration of $\text{CuCr}_{0.99}\text{Ln}_{0.01}\text{S}_2$ ($\text{Ln} = \text{Dy-Lu}$). *Materials* **2023**, *16*, 2431. [[CrossRef](#)] [[PubMed](#)]
34. Korotaev, E.V.; Syrokvashin, M.M.; Filatova, I.Y.; Zvereva, V.V. Magnetic Properties of Novel Layered Disulfides $\text{CuCr}_{0.99}\text{Ln}_{0.01}\text{S}_2$ ($\text{Ln} = \text{La} \dots \text{Lu}$). *Materials* **2021**, *14*, 5101. [[CrossRef](#)] [[PubMed](#)]
35. Korotaev, E.V.; Syrokvashin, M.M.; Filatova, I.Y.; Kalinkin, A.V.; Sotnikov, A.V. Valence band structure and charge distribution in the layered lanthanide-doped $\text{CuCr}_{0.99}\text{Ln}_{0.01}\text{S}_2$ ($\text{Ln} = \text{La}, \text{Ce}$) solid solutions. *Sci. Rep.* **2021**, *11*, 18934. [[CrossRef](#)]
36. Korotaev, E.V.; Syrokvashin, M.M.; Filatova, I.Y.; Sotnikov, A.V.; Kalinkin, A.V. Charge Distribution in Layered Lanthanide-Doped $\text{CuCr}_{0.99}\text{Ln}_{0.01}\text{S}_2$ ($\text{Ln} = \text{Pr-Tb}$) Thermoelectric Materials. *Materials* **2022**, *15*, 8747. [[CrossRef](#)]
37. Mori, T.; Maignan, A. Thermoelectric materials developments: Past, present, and future. *Sci. Technol. Adv. Mater.* **2021**, *22*, 998–999. [[CrossRef](#)]
38. Tsujii, N.; Kitazawa, H. Substitution effect on the two-dimensional triangular-lattice system CuCrS_2 . *J. Phys. Condens. Matter* **2007**, *19*, 145245. [[CrossRef](#)]
39. Korotaev, E.V.; Syrokvashin, M.M.; Filatova, I.Y.; Zvereva, V.V. Vanadium doped layered copper-chromium sulfides: The correlation between the magnetic properties and XES data. *Vacuum* **2020**, *179*, 109390. [[CrossRef](#)]
40. Hollander, J.C.T.; Sawatzky, G.; Haas, C. Monovalent copper in the chalcogenide spinel CuCr_2Se_4 . *Solid. State Commun.* **1974**, *15*, 747–751. [[CrossRef](#)]
41. Mazalov, L.N.; Sokolov, V.V.; Kryuchkova, N.A.; Vovk, E.I.; Filatova, I.Y.; Abramova, G.M. X-ray photoelectron spectroscopic studies of the charged state of 3d metal ions in $\text{CuCr}_{1-x}\text{V}_x\text{S}_2$ ($x = 0-0.4$). *J. Struct. Chem.* **2009**, *50*, 439–445. [[CrossRef](#)]
42. Korotaev, E.V.; Syrokvashin, M.M.; Sulyaeva, V.S.; Filatova, I.Y. Magnetic Properties of $\text{CuCr}_{1-x}\text{La}_x\text{S}_2$ Thermoelectric Materials. *Magnetochemistry* **2023**, *9*, 168. [[CrossRef](#)]
43. CasaXPS Software. Available online: <http://www.casaxps.com/> (accessed on 14 November 2022).
44. Inorganic Crystal Structure Database, Version 2.1.0; Leibniz Institute for Information Infrastructure, FIZ Karlsruhe: Eggenstein-Leopoldshafen, Germany. Available online: <https://icsd.products.fiz-karlsruhe.de/> (accessed on 17 August 2021).

45. Shalimova, K.V. *Semiconductors Physics*; Lan: St. Petersburg, Russia, 2021; ISBN 978-5-8114-0922-8.
46. Kabongo, G.L.L.; Mhlongo, G.H.H.; Mothudi, B.M.M.; Hillie, K.T.T.; Mbule, P.S.S.; Dhlamini, M.S.S. Structural, photoluminescence and XPS properties of Tm 3+ ions in ZnO nanostructures. *J. Lumin.* **2017**, *187*, 141–153. [[CrossRef](#)]
47. de Groot, F.; Kotani, A. *Core Level Spectroscopy of Solids*; CRC Press: Boca Raton, FL, USA, 2008; ISBN 9780429195792.
48. Larsson, S. Satellites in ESCA inner-shell spectra of 3d0 transition metal complexes. *J. Electron. Spectros. Relat. Phenom.* **1976**, *8*, 171–178. [[CrossRef](#)]
49. Vasil'eva, I.G.; Kriventsov, V.V. Structural Study of CuCr1-XVxS2 Substitutional Solid Solutions. *J. Surf. Investig.* **2010**, *4*, 640–644. [[CrossRef](#)]
50. NIST X-ray Photoelectron Spectroscopy (XPS) Database, Version 3.5. Available online: <https://srdata.nist.gov/xps/> (accessed on 14 November 2022).
51. XPS, AES, UPS and ESCA Database. Available online: <http://www.lasurface.com/database/elementxps.php> (accessed on 14 November 2022).
52. Starodub, V.A. Ternary and Quaternary Chalcogenides of Group IB Elements. *Usp. Khim.* **1999**, *68*, 902–903. [[CrossRef](#)]
53. Mikhlin, Y.L.L.; Tomashevich, Y.V.V.; Pashkov, G.L.L.; Okotrub, A.V.V.; Asanov, I.P.P.; Mazalov, L.N.N. Electronic structure of the non-equilibrium iron-deficient layer of hexagonal pyrrhotite. *Appl. Surf. Sci.* **1998**, *125*, 73–84. [[CrossRef](#)]
54. Mikhlin, Y.; Karacharov, A.; Vorobyev, S.; Romanchenko, A.; Likhatski, M.; Antsiferova, S.; Markosyan, S. Towards Understanding the Role of Surface Gas Nanostructures: Effect of Temperature Difference Pretreatment on Wetting and Flotation of Sulfide Minerals and Pb-Zn Ore. *Nanomaterials* **2020**, *10*, 1362. [[CrossRef](#)] [[PubMed](#)]
55. Selwood, P. *Magnetochemistry*, 2nd ed.; Interscience Publishers: New York, NY, USA, 1956.
56. Blundell, S. *Magnetism in Condensed Matter*; OXFORD University Press: Oxford, UK, 2001. [[CrossRef](#)]
57. Le Nagard, N.; Collin, G.; Gorochoy, O. Etude structurale et proprietes physiques de CuCrS2. *Mater. Res. Bull.* **1979**, *14*, 1411–1417. [[CrossRef](#)]
58. Abramova, G.M.; Petrakovskij, G.A.; Vorotynov, A.M.; Velikanov, D.A.; Kiselev, N.I.; Bovina, A.F.; Szymczak, R.; Al'mukhametov, R.F. Phase transitions and colossal magnetoresistance in CuVxCr 1-x S2 layered disulfides. *JETP Lett.* **2006**, *83*, 118–121. [[CrossRef](#)]

Disclaimer/Publisher's Note: The statements, opinions and data contained in all publications are solely those of the individual author(s) and contributor(s) and not of MDPI and/or the editor(s). MDPI and/or the editor(s) disclaim responsibility for any injury to people or property resulting from any ideas, methods, instructions or products referred to in the content.